

# The optical/UV excess of X-ray-dim isolated neutron star.

## II. Nonuniformity of plasma on strangeon star surface

W. Y. Wang<sup>1,2,3\*</sup>, Y. Feng<sup>2,4</sup>, X. Y. Lai<sup>5</sup>, Y. Y. Li<sup>3</sup>, J. G. Lu<sup>3</sup>, X. L. Chen<sup>1,2,6</sup>, R. X. Xu<sup>3,7</sup>

<sup>1</sup>Key Laboratory of Computational Astrophysics, National Astronomical Observatories, Chinese Academy of Sciences, Beijing 100012, China

<sup>2</sup>School of Astronomy and Space Sciences, University of Chinese Academy of Sciences, Beijing 100049, China

<sup>3</sup>School of Physics and State Key Laboratory of Nuclear Physics and Technology, Peking University, Beijing 100871, China

<sup>4</sup>National Astronomical Observatories, Chinese Academy of Sciences, Beijing, China

<sup>5</sup>Hubei University of Education, Wuhan 430205, China

<sup>6</sup>Center for High Energy Physics, Peking University, Beijing 100871, China

<sup>7</sup>Kavli Institute for Astronomy and Astrophysics, Peking University, Beijing 100871, China

Accepted XXX. Received YYY; in original form ZZZ

### ABSTRACT

X-ray-dim isolated neutron stars (XDINSs), also known as the Magnificent Seven, exhibits a Planck-like soft X-ray spectrum. In the optical/ultraviolet (UV) band, there is an excess of radiation compared to the extrapolation from the X-ray spectrum. However, the majority exhibit “spectral deviations”: the fact that there are more flux at longer wavelengths makes spectra deviating from Rayleigh-Jeans laws. A model of bremsstrahlung emission from a nonuniform plasma atmosphere is proposed in the regime of a strangeon star to explain the optical/UV excess and its spectral deviation as well as X-ray pulsation. The atmosphere is on the surface of emission-negligible strangeon matter, formed by the accretion of interstellar matter moving along the magnetic field lines to polar caps, and these particles may spread out of the pole regions that makes the atmosphere non-uniform. The modeled electron temperatures are  $\sim 100 - 200$  eV with radiation radii  $R_{\text{opt}}^{\infty} \sim 5 - 14$  km. The spectra of five sources (RX J0720.4–3125, RX J0806.4–4123, RX J1308.6+2127, RX J1605.3+3249, RX J1856.5–3754) from optical/UV to X-ray bands could be well fitted by the radiative model, and exhibit gaussian absorption lines at  $\sim 100 - 500$  eV as would be expected. Furthermore, the surroundings (i.e., fallback disks or dusty belts) of XDINSs could be tested by future observations with the Large Optical Telescope (LOT).

**Key words:** X-rays: stars – stars: neutron – stars: individual

### 1 INTRODUCTION

The Magnificent Seven refers to seven X-ray-dim isolated neutron stars (XDINSs) with thermal radiation of soft X-rays, which offer an unprecedented opportunity to unveil their surface temperature and magnetic field as well as the state of dense matter at supra nuclear densities (Turolla 2009). These objects, RX J1856.5–3754 (J1856 hereafter as other sources) for instance, are characterized by Planck-like spectra (no power law component) in the X-ray band with a relatively steady flux over long timescales (Burwitz et al. 2001; Ho et al. 2007; van Kerkwijk & Kaplan 2007; Kaplan & van Kerkwijk 2009). They are located in the upper right corner of  $P - \dot{P}$  diagram together with a few high- $B$  pulsars and magnetars, indicating that they may have strong magnetic fields (Mori & Ruderman 2003; Tong

2016). However, if they are normal neutron stars, the strong magnetic field should give rise to significant absorption lines in the thermal spectrum (e.g., Suleimanov et al. 2010), but the X-ray spectra of XDINS such as J1856 are almost featureless. Additionally, compared with the extrapolated blackbody X-ray spectrum, the XDINS exhibits an excess in optical/UV flux, with a factor of  $\sim 5 - 50$  (Kaplan et al. 2011). To explain this, one can adopt a two-component blackbody radiative model. In the case of J1856 (at a distance  $d \sim 120$  pc from us), for example, the temperature of the hot component is  $kT_{\text{X}}^{\infty} \sim 63.5$  eV with radiation radius  $R_{\text{X}}^{\infty} \sim 4.4 (d/120 \text{ pc}) \text{ km}$ , while that of the cold part is  $kT_{\text{opt}} < 33$  eV ( $R_{\text{opt}}^{\infty} > 17 (d/120 \text{ pc}) \text{ km}$ ) (Burwitz et al. 2003; Trümper et al. 2004). The fact that the radiation radius is smaller than that of a typical neutron star and the featureless blackbody spectrum leads to the suggestion that J1856 and other XDINSs might be strange quark stars or strangeon stars (Haensel 2001; Drake et al. 2002; Xu 2002,

\* E-mail: wywang@bao.ac.cn

2003; for a general introduction to strangeon star, see, Lai & Xu 2017). Heretofore in this paper, we will refer to all pulsar-like compact objects as NS, regardless of whether they are composed of neutrons or strangeon.

A bremsstrahlung radiative model of a strangeon star atmosphere was proposed to explain the optical/UV excess (Wang et al. 2017). The atmosphere is modeled with two temperature components (Xu 2014), formed by accretion of interstellar medium, and can be simply considered as the upper layer of a normal NS. The radiation is optically thick at optical bands while optically thin at X-ray bands. Thus, the observed spectra of the Seven could be well fitted by the radiative model, from optical to X-ray bands. The radiation radii of XDINSs in this model are from 3 to 13 km, while the temperature of electrons are between 50 and 250 eV.

However, it is *not an alleged* observation that the optical flux appears to deviate from a Rayleigh-Jeans (R-J) distribution. The spectrum can be described as a power law emission ( $F_\nu \propto \nu^\beta$ ). For R-J spectrum  $\beta = 2$ , but the spectra for XDINS are flatter (Kaplan et al. 2011) with the only exception of RX J0420.0–5022. Alternatively, Ertan et al. (2017) proposed that magnetic work can heat up the inner disc matter which is expected to bring much low energy photons. Also noteworthy is the fact that the spectral deviations of most XDINSs are greater than the photoelectric absorptions by neutral hydrogen as modeled from X-ray spectra. Certainly, more powerful observations would make sure if the deviations are real, but we are focusing to understand the flat spectrum here.

In this paper, we propose that the spectral deviations come from non-uniformities of the atmosphere which is on top of an emission-negligible strangeon star surface. The accreted interstellar matter moves along the magnetic field lines to polar caps of the NS, and parts of them may diffuse to other regions, generating a nonuniform distribution of the atmosphere. Thus, the spectrum may deviate from a R-J radiation at optical bands because the bremsstrahlung emissivity is particle distribution-dependent (as demonstrated in Fig. 2).

In section 2.1, we interpret that the strangeon matter could be emission-negligible. In Section 2.2, we propose a toy model to describe the non-uniformity of the atmosphere and show that this distribution could make the spectrum deviating from the R-J regime. In Section 3, we present the fitting details and results for the X-ray data (Sec. 3.1) and optical data (Sec. 3.2). Finally, we discuss various issues in this model in Section 4, and make a brief summary in Section 5.

## 2 RADIATION FROM A STRANGEON STAR

### 2.1 Emission from the strangeon star surface

The radiation from strangeon matter is totally neglected in the calculation as following, and this could be valid because of the high plasma frequency,  $\omega_p$ . The plasma frequency of degenerated charged Fermion gas,  $\omega_p \propto n^{1/3}$ , with  $n$  the number density (Usov 2001). For strangeon matter with baryon density,  $n_b$ , to be a few nuclear density, the electron number density  $n_e = (10^{-5} \sim 10^{-6})n_b$ , with baryon number density  $n_b = (1.5 - 2.0)n_{\text{nuc}}$ , where  $n_{\text{nuc}}$  is the normal nuclear matter density (Alcock et al. 1986), and then

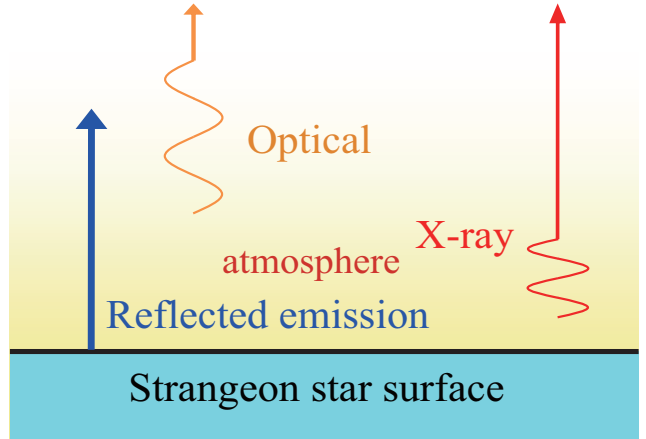


**Figure 1.** A schematic diagram of the observed radiation from the atmosphere which is on top of a strangeon star. The total observed radiation consists of the emission from the atmosphere and the reflected component by the emission-negligible surface. The radiation is optically thin at X-ray bands so that photons can emit from much deeper location, while optically thick for long wavelength photons.

the frequency  $\omega_p \sim 100$  keV is so high that the optical as well as soft X-ray emissivity is negligible. Therefore, the strangeon star's atmosphere could be similar to the upper layer of a normal NS, but there do exist differences (Fig 1). The emission-negligible surface does not bring a lot of high energy photons that is coincidence with the fact of the high energy tail absence in the X-ray spectrum of XDINS (e.g., van Kerkwijk et al. 2007).

However, the strangeon matter surface exhibit an extremely high reflectance that can be regarded as total reflection. The reflected component by the strangeon matter surface should certainly be included in the total emission. Then, the observed flux is multiplied by a factor of  $[1 + \exp(-\tau_\infty)]$ , where the factor of  $\exp(-\tau_\infty)$  results from the reflection (see Appendix) and illustrated in Figure 1. The reflection effect intensifies X-ray emissions while can be ignored in optical bands.

### 2.2 The plasma atmosphere with non-uniformity: A toy model

A nonuniform plasma atmosphere could produce a bremsstrahlung radiation spectrum deviating from the R-J law at low energy (optical/UV) bands, because the optical depth of the radiation is energy-dependent (Wang et al. 2017). The total flux is the sum of radiation from local regions (see Equation (11) in Appendix). In these cases, a nonuniform atmosphere may enable the spectral index to deviate from a R-J spectrum. A sample of deviated spectra from a nonuniform atmosphere are shown in Figure 2. It is worth noting that the radiation in high energy is mainly from the polar caps. Therefore, the data of both high energy and low energy can be fitted separately (see Section 3). Actually, the observed flux is the time-averaged radiation from a rotating NS and the detailed calculations are shown in the Appendix.

It is worth noting that the temperature gradient could not be the reason for the deviation because of the high ther-

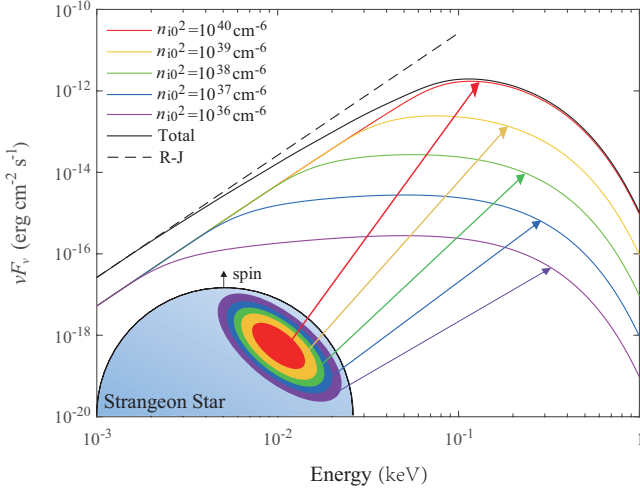


**Figure 2.** The observed spectrum of a rotating NS with a nonuniform atmosphere. The total radiation consists of five components with same radiative areas while different number density:  $n_{i0}^2 = 10^{40} \text{ cm}^{-6}$  (red solid line),  $n_{i0}^2 = 10^{39} \text{ cm}^{-6}$  (yellow solid line),  $n_{i0}^2 = 10^{38} \text{ cm}^{-6}$  (green solid line),  $n_{i0}^2 = 10^{37} \text{ cm}^{-6}$  (blue solid line) and  $n_{i0}^2 = 10^{36} \text{ cm}^{-6}$  (purple solid line), for given  $T_e = 0.1 \text{ keV}$ ,  $T_i = 0.1 \text{ MeV}$  and  $(R_{\text{opt}}^\infty/d)^2 = (10 \text{ km}/0.25 \text{ kpc})^2$ . The total radiation (the black solid line) of these five components exhibits a deviation compared with a R-J spectrum (dotted line).

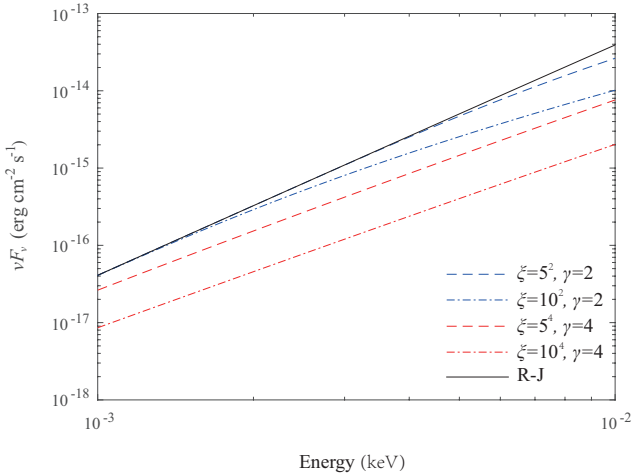


**Figure 3.** Comparison of photo indexes of the spectrum with  $\xi = 5$ , including  $\gamma = 2$  (blue dashed line) and  $\gamma = 4$  (red dashed line), and the corresponding case  $\xi = 10$  with  $\gamma = 2$  (blue dashed-dotted line) and  $\gamma = 4$  (red dashed-dotted line). The solid line is a R-J spectrum from a uniform atmosphere.

mal conductivity of the star surface unless there is an extremely strong magnetic field ( $\sim 10^{15} \text{ G}$ , e.g., Pons et al. 2009). Thus, we regard the non-uniformity of the number density as the main reason for the fact of spectral index deviation. However, a Goldreich-Julian-like distribution (Goldreich & Julian 1969) in a dipolar magnetic field cannot explain the deviation because the regions which have low density radiative matters are very small. There are some possible reasons for the non-Goldreich-Julian-like distribution: i) some atmospheric matter gyrate around the magnetic lines

**Table 1.** Summary of Photometry and some parameters for XDINSs

Source	Optical (mag)	$\beta$	$\xi (\times 10^2)$	$\gamma$	PF (%)
J0420	$B = 26.6$	$2.20 \pm 0.22$	—	—	13
J0720	$B = 26.6$	$1.43 \pm 0.12$	2.5	5	8–15
J0806	$B > 24$	$1.63 \pm 0.20$	1.5	3	6
J1308	$m_{50\text{ccd}} = 28.6$	$1.62 \pm 0.14$	0	—	18
J1605	$B = 27.2$	$1.23 \pm 0.07$	5.0	3	—
J1856	$B = 25.2$	$1.93 \pm 0.08$	0	—	<1.3
J2143	$B > 26$	$0.53 \pm 0.08$	> 1	> 1	4

**Notes.** The optical data quoted from Kaplan et al. (2011) of each XDINS can be fitted by a power law ( $F_\nu \propto \nu^\beta$ , where  $\beta$  is the photo index). The optical stellar magnitude and pulsed fraction (PF) shown in this table are quoted from Haberl 2007.

and diffuse to other regions; ii) there are some multipolar magnetic fields that support particles moving into high latitude regions from polar caps.

As we have discussed in Sec 2.1, the atmospheric matter is accreted by gravity and moves along the magnetic field lines to polar caps. However, there may be some multipolar magnetic fields that help small parts of the accreted matters spread out of the polar caps exhibiting a nonuniform particle distribution. Here, based on the above analysis, it is assumed that the atmosphere: i) is approximately uniform at polar caps; ii) can be described by a power-law-like distribution at high latitudes; iii) decreases rapidly at the edges of polar caps. To simply account the complicated atmospheric distribution in the magnetosphere, we propose a toy model to describe the nonuniformity. An assumed distribution of number density can be constructed,

$$n_e = n_i = n_{i0}(\theta) \exp\left(\frac{-m_i g z}{k T_i}\right) = n_0 \frac{\exp\left(\frac{-m_i g z}{k T_i}\right)}{1 + \xi \cdot \theta^\gamma}, \quad (1)$$

where  $z$  measures the height above the star's surface,  $n_0$  is the number density of ions on the star's surface at  $\theta = 0$ ,  $m_i$  is the mass of a ion (mainly proton),  $T_i$  is the temperature of ions,  $g$  is the gravitational acceleration above the surface of a strangeon star, and  $\xi$  as well as  $\gamma$  are two constants to describe the nonuniformity, respectively. The rationalities of the toy model are discussed in Section 4.2. In this case, the plasma atmosphere would be approximately uniform if all the ISM-accreted matter can diffuse from the polar caps to other parts of the stellar surface (i.e.,  $\xi = 0$ , where a Rayleigh-Jeans spectrum is shown at optical bands). In order to show the impacts of  $\xi$  and  $\gamma$  on the spectral index, we calculate the observed time-averaged spectrum with  $k T_e = 0.1 \text{ keV}$ ,  $n_0^2 k T_i = 10^{42} \text{ keV cm}^{-6}$ ,  $(R_{\text{opt}}^\infty/d)^2 = (10 \text{ km}/0.25 \text{ kpc})^2$ ,  $\zeta = 0$  and  $\alpha = 0$  (definition of  $\zeta$  and  $\alpha$ , see Appendix). The comparison of deviation with different  $\xi$  and  $\gamma$  is shown in Figure 3.

### 3 DATA REDUCTION AND FITTING

#### 3.1 X-ray data

The details of X-ray data reduction from *XMM-Newton* for the Seven can be seen in Wang et al. (2017). The XDINS

spectral analysis is performed with XSPEC 12.9 (Arnaud 1996), selecting photon energies in the range of 0.1–1.0 keV. To omit some degeneracies, two angles  $\zeta$  and  $\alpha$  are treated as zero because the spectra are not going to be felt in the range of  $\zeta < 30^\circ$  and  $\alpha < 15^\circ$ . In addition, there is little decrease for flux with  $\zeta$  and  $\alpha$  increasing while not for the spectral index.

The optical and X-ray data can be fitted separately because the emission is optically thin at high-energy bands while optically thick at optical bands. We first fit X-ray data with the uniform atmosphere model accounting for polar caps mainly emit high energy photons. The results of spectral fitted by the uniform model with absorption lines are presented in Wang et al. (2017). Therefore, we fix  $N_H$ ,  $T_e$  and  $E_{\text{Line}}$  as the modelled uniform atmosphere while command  $y/R$  (where  $y = n_{i0}^2 kT_i$ ,  $R$  is assumed to be  $R_{\text{opt}}^\infty$ ) and width  $\sigma$  as free parameters. And then we treat all these fixed parameters as free, and extract the best-fit  $N_H$  to fix photoelectric absorption.

The optical data are fitted by the absorbed nonuniform radiative model with free  $R_{\text{opt}}^\infty$  as well as fixed  $\xi$  and  $\gamma$  which are reported in Table 1 (details, see Section 3.2). Then, with modelled  $R_{\text{opt}}^\infty$ , the X-ray data are fitted by the nonuniform model. The best modeled values and errors of parameters are presented in Table 2. With these parameters, the radiative spectra and spectral data of J0720, J0806, J1308, J1605 and J1856 are reproduced and plotted in Figure 4. The X-ray data are also fitted by the blackbody model while only J1856 shows a better fit ( $\chi^2 = 1.11$ ) than the bremsstrahlung emission.

### 3.2 Optical data

Optical counterparts for each XDINS have been searched in deep optical observations by *HST*, and detailed photometry measurements and data errors are presented in Kaplan et al. (2011). Each photometry spectrum of XDINS can be fitted by a power law and fixed by a function of extinction in which the value is determined by the column density of hydrogen  $N_H$  from X-ray spectrum data fitting (details of XSPEC photoelectric absorption are shown in Morrison & McCammon 1983).

To describe a photoelectric absorption when the light transmitting through an extinction layer, the atmospheric extinction in magnitudes  $A_\lambda$  is defined (see, Cardelli & Ackerman 1983, Equation (3)), and optical extinction  $A_V$  depends on  $N_H$  which is given by X-ray spectral fitting:  $A_V = N_H / 1.79 \times 10^{21} \text{ cm}^{-2}$  (Predehl & Schmitt 1995). In general, the extinction value  $A_\lambda/A_V$  depends on wavelength and the value of the overall extinction  $A_V$ . However,  $A_\lambda/A_V$  can be considered as wavelength-dependent since the changes are less than 1% in  $A_\lambda/A_V$  for the range of  $N_H = (1-4) \times 10^{20} \text{ cm}^{-2}$  (Kaplan et al. 2011). The absorbed flux can be described as

$$F_\nu = F_{\nu 0} \cdot 10^{-2.23 \frac{A_\lambda}{A_V} \cdot \frac{N_H}{10^{22} \text{ cm}^{-2}}},$$

where  $F_{\nu 0}$  is the unabsorbed flux. van Kerkwijk & Kulkarni (2001a) presents a approximate wavelength-dependent values of  $A_\lambda/A_V$  for an unabsorbed  $10^6 \text{ K}$  ( $\sim 100 \text{ eV}$ ) blackbody.

Then, with fixed photoelectric absorption, the optical data are fitted by the nonuniform radiative models. In

this process,  $R_{\text{opt}}^\infty$  is treated as a free parameter while  $\xi$  and  $\gamma$  are fixed. Therefore, the spectra of J1308 and J1856 can be well fitted by R-J-like emissions which are photoelectric absorbed without nonuniformity. For J1605, X-ray data fitting with a uniform radiative model presents a large value of  $N_H \sim 3 \times 10^{20} \text{ cm}^{-2}$ . In this case, the absorbed nonuniform emission can well fit the deviate spectrum. However, the nonuniform radiation predicts that  $N_H$  would be smaller than  $\sim 1.5 \times 10^{20} \text{ cm}^{-2}$  because the nonuniformity of the atmosphere decreases the emissions from polar caps in low-energy X-ray bands ( $\sim 0.1 - 0.4 \text{ keV}$ ). The same case for J0806 that  $N_H$  is estimated to be  $\sim 2.2 \times 10^{20} \text{ cm}^{-2}$ , which is supposed to be smaller than Galactic value  $2.7 \times 10^{20} \text{ cm}^{-2}$  obtained from Kalberla et al. (2005). While J1308 shows a larger value of  $N_H$  that may indicates a long distance from us or a much denser interstellar surrounding. The observation of this source shows a high PF ( $\sim 18\%$ , Kaplan & van Kerkwijk 2005) that leads to large fitting errors, and the gravitational redshift of this source is  $\sim 0.16$  which demonstrates  $(M/M_\odot)/(R/1 \text{ km}) \sim 0.87$  indicating a stiff equation of state of NS (Potekhin et al. 2016).

The faintest X-ray source among the Seven, J0420, shows a steeper spectrum ( $\beta = 2.20 \pm 0.22$  which is greater than the case of R-J regime) at optical/UV bands that is different with other XDINSs. This large photo index may result from the large value of PF (a factor of  $\sim 13\%$ ) which is revealed by fitting a sine wave to the X-ray pulse profile (Haberl et al. 2004). The data and spectral fitting by the uniform atmosphere model of J0420 and J2143 are reproduced and plotted in Figure 5. In addition, J2143 shows a flatter optical spectrum ( $\beta = 0.53 \pm 0.08$ ). One possible reason for the flat spectra is that a strong magnetic field ( $\gtrsim 10^{15} \text{ G}$ , e.g., Pons et al. 2009) blocks atmospheric matters making them diffuse hardly. In this case, the temperature gradient should be considered (similar like a multi-color blackbody spectrum of a black hole accretion disk which presents a spectral index  $\sim 0.33$  at low energy bands). Or there may be a high toroidal magnetic field that blocks transmission of heat (Geppert et al. 2006). Almost all of the accreted matter cannot spread out from the small pole regions that also demonstrate an extremely thin atmosphere. We use an uniform radiative model with an absorption edge and a Gaussian absorption to fit the X-ray data of J2143. The best fitted result shows two absorptions  $E_{\text{edge}} = 365.6 \pm 2.2 \text{ eV}$  with  $\tau = 1.07 \pm 0.07$  and  $E_{\text{Gaus}} = 759.0 \pm 11.1 \text{ eV}$ . These absorptions may predict a strong magnetic field.

We list the values of  $\xi$  and  $\gamma$  that are at  $\geq 1\sigma$  confidence in Table 1 and the modelled  $R_{\text{opt}}^\infty$  in Table 2. Five of the Seven spectra could be well fitted by the radiative model, from optical/UV to X-ray bands, exhibit absorption lines (discussions of these lines can be seen in Wang et al. 2017). In addition, we plot the absorbed bremsstrahlung and blackbody radiations to demonstrate the optical/UV excess of XDINS (see Figure 4).

## 4 DISCUSSION

### 4.1 The accretion and evolution of the XDINS

In a generalized ISM-fed debris disk accretion (IFDA) model, NS accretes from a thin fall-back disk in the early

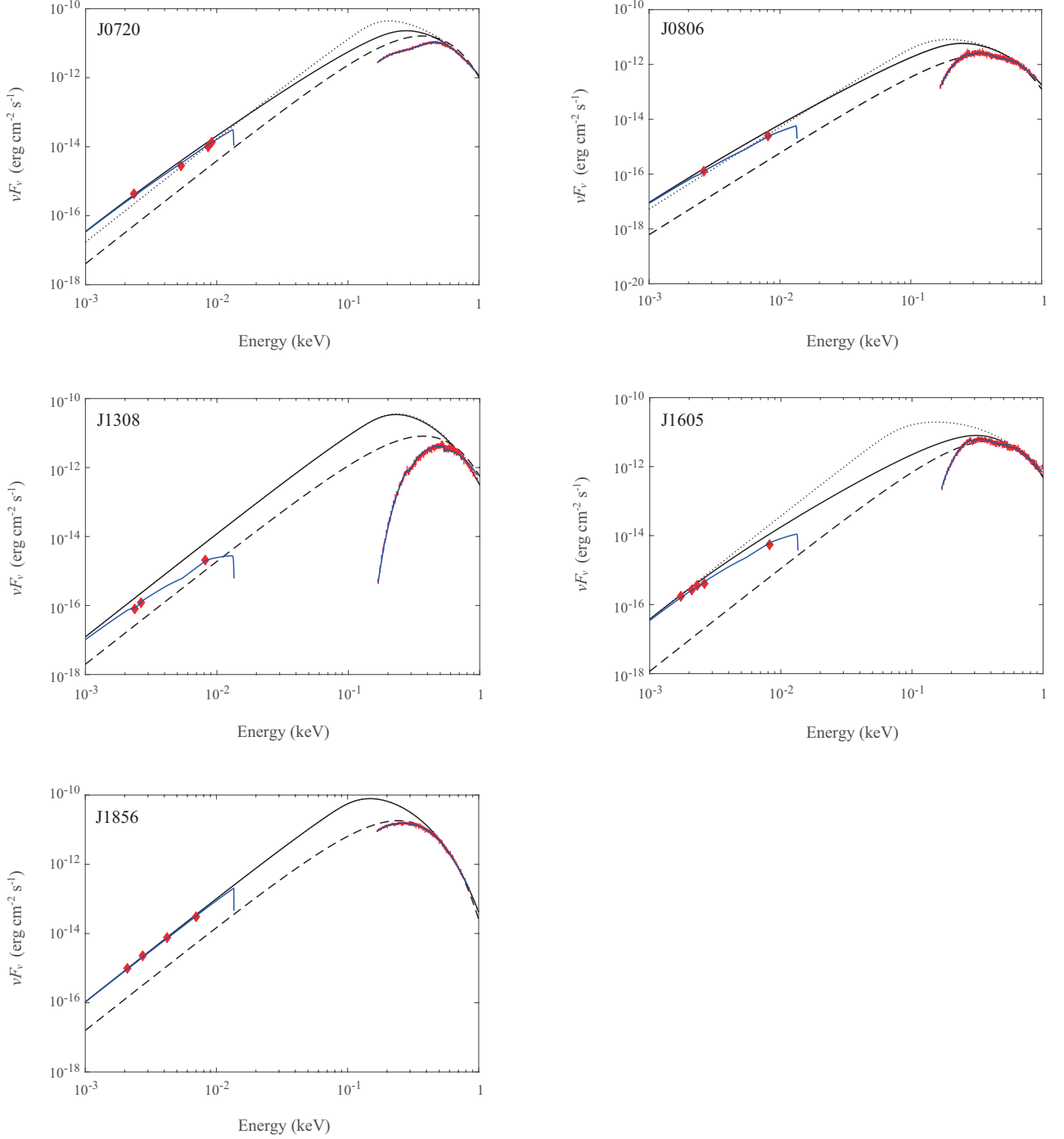


**Figure 4.** The spectra of J0720(top left), J0806(top right), J1308(center left), J1605(center right) and J1856 (bottom) from optical to X-ray bands are shown in this figure. The absorbed best-fit nonuniform radiative model of each source is the blue solid line, while the unabsorbed nonuniform radiative model is the black solid line. To exhibit the optical/UV excesses, pure blackbody (black dashed line) extrapolated from each X-ray spectrum are plotted. The archival X-ray data with their error bars from *XMM-Newton* (red dot) and optical data (red diamond) from *HST* are also plotted. By comparison, the uniform radiative model (black dotted line) is also plotted.

phase through the propeller mechanism and transform to a thick disk accretion or spherical accretion in the late phase as the disk depletes and the ISM dominate the accretion. It is worth noting that XDINSs are regarded as be in stage of a “transitional” accretion mode. In this mode, a thin disk accretion (i.e., propeller phase) dominates the evolution of NS

while the geometry of the disk is supposed be thick because of the ISM supplement and disk depleting.

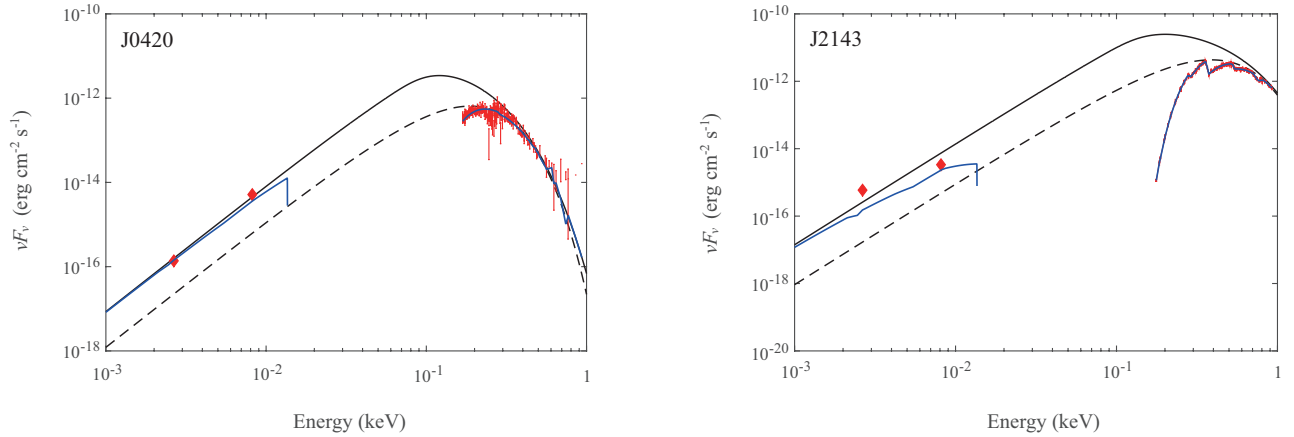
The radiation is supposed to come from the accreted-ISM matter on the stellar surface instead of the disk. As a magnetic ISM-accreted NS, the X-ray luminous accreted matter is a small fraction of the disk incoming matter. Thus, the accretion rate at Alfvén radius  $\dot{M}_A$  should be larger than



**Table 2.** The parameters obtained from X-ray spectral fitting

Source RX	$kT_e$ (eV)	$R_{\text{opt}}^\infty$ (km)	$y$ ( $\times 10^{42} \text{ cm}^{-6} \text{ keV}$ )	Absorption (eV)	$N_H$ ( $\times 10^{20} \text{ cm}^{-2}$ )	$d$ (pc)	$\chi^2/\text{dof}$
J0420.0–5022	$71.6 \pm 2.5$	$9.3 \pm 0.3$	$1.49 \pm 0.25$	250	$1.60 \pm 0.47$	345	1.15/131
J0720.4–3125	$179.0 \pm 2.2$	$13.5 \pm 0.1$	$37.3 \pm 2.21$	$217.8 \pm 20.3$	$1.02 \pm 0.33$	360	1.43/199
J0806.4–4123	$165.8 \pm 5.8$	$4.5 \pm 0.2$	$5.00 \pm 0.82$	$445.8 \pm 4.3$	$3.26 \pm 0.19$	250	1.01/423
J1308.6+2127	$131.4 \pm 2.4$	$12.0 \pm 0.2$	$10.46 \pm 1.13$	$408.9 \pm 3.4$	$8.77 \pm 0.19$	500	1.05/285
J1605.3+3249	$181.1 \pm 6.5$	$13.9 \pm 0.5$	$1.12 \pm 0.18$	$445.2 \pm 4.7$	$3.28 \pm 0.18$	390	1.12/320
J1856.5–3754	$96.2 \pm 1.1$	$12.8 \pm 0.1$	$2.11 \pm 0.15$	$110.5 \pm 56.9$	$0.68 \pm 0.26$	160	1.13/297
J2143.0+0654	$158.0 \pm 3.7$	$11.7 \pm 0.2$	$10.37 \pm 1.29$	$759.0 \pm 11.1$	$8.36 \pm 2.41$	430	1.14/225

**Notes.** Columns 1 – 8 are source name (“Source RX”), temperature of electrons (“ $kT_e$ ”), radius of stars (“ $R_{\text{opt}}^\infty$ ”), parameter  $y$ , absorption lines, neutral hydrogen column density (“ $N_H$ ”), distance (“ $d$ ”) and  $\chi^2/\text{degree of freedom}$ . Errors on the spectral model parameters are derived for a 90% confidence level. The distances are from [Kaplan & van Kerkwijk \(2009\)](#). The absorption model is Gaussian function and that for J0420 is fixed. J2143 also shows an edge at  $E_{\text{edge}} = 365.6 \pm 2.2 \text{ eV}$  with  $\tau = 1.07 \pm 0.07$ .

**Figure 5.** Same as Figure 4 but for J0420(left) and J2143(right). The uniform radiative model is the black solid line.

the X-ray luminous accretion rate  $\dot{M}_X \sim 10^{10} - 10^{11} \text{ g/s}$  with a value of  $10 - 100$  ([Toropin et al. 2001](#)). The Alfvén radius  $R_A = (\frac{R^6 B^2}{M_A \sqrt{2GM}})^{2/7} \lesssim 10^{10} \text{ cm}$  and the Bondi radius  $R_B \sim 10^{12} \text{ cm}$  can be calculated ([Wang et al. 2017](#)). For such slowly rotating NS, the light cylinder radius is calculated to be  $R_{\text{LC}} \sim 10^{10} \text{ cm}$ . In case of  $R_A < R_{\text{LC}} < R_B$ , the ISM matter would be accreted along the magnetic field lines to polar caps. The inflow matters can be observed both in simulations of ISM-accreted propeller and disk accretion propeller ([Romanova et al. 2003, 2017](#)). And these matters is sufficient to maintain the radiation. In addition, considering the thermal equilibrium at  $R_A$ , the luminosity at  $R_A$  is  $L_A = (3/2)GM\dot{M}_A/R_A = 10^{27-28} \text{ erg/s}$ . The effective temperature can be estimated to be  $T_A = [L_A/(4\pi R_A^2 \sigma)]^{1/4} \sim 0.1 \text{ eV}$ . In this case, the contribution from the disk to the optical/UV emission (X-ray as well) can be ignored.

With the magnetospheric radius  $\sim R_A$  is larger than the corotation radius  $R_{\text{Co}} = (GM/\Omega)^{1/3} \sim 10^8 \text{ cm}$ , the NS is in a so-called “propeller” stage ([Davidson & Ostriker 1973; Illarionov & Sunyaev 1975](#)). Thus, one can obtain the braking torque ([Menou et al. 1999; Chatterjee et al. 2000](#))

$$N = 2\dot{M}_A R_A^2 \Omega_K(R_A) [1 - \frac{\Omega}{\Omega_K(R_A)}], \quad (2)$$

where  $\Omega$  is the angular frequency of NS and  $\Omega_K(R_A) = \sqrt{GM/R_A^3}$  is the Kepler angular frequency at  $R_A$ . The spin-down rate  $\dot{P} \sim 10^{-14} \text{ ss}^{-1}$  is consistent with the observa-

tion. In this case, the spin-down timescale is estimated to be  $\sim 10^6$  years.

## 4.2 Nonuniformity of the atmosphere

In Section 2.2, we propose that a nonuniform atmosphere would lead to the spectral index deviation. If this deviation is originated from the temperature gradient (e.g., two component of blackbody), there would be a lower temperature  $T \lesssim 10^5 \text{ K}$  component that deviates from the calculation of a low thermal conductivity on a star surface. One possible reason is a high crustal toroidal magnetic field  $B_{\text{tor}} \sim 10^{15} \text{ G}$  that blocks the heating transform ([Geppert et al. 2006](#)). In terms of the nondeviate optical spectrum (i.e., R-J spectrum), the observed optical depth  $\tau_\infty \gtrsim 1$  at  $\sim 10 \text{ eV}$  that leads to the surface number density  $n_{i0}(\theta) \gtrsim 10^{17} \text{ cm}^{-3}$ . In fact, falling atoms move along the magnetic field lines to the polar caps, and collisions between the ions and electrons may make them diffuse across the magnetic field lines. The atmosphere would be spherically symmetrical (i.e., uniform) if these charged particles could quickly spread around the whole surface.

In case of the Seven rotate slowly, the diffusion of these charged atmospheric particles can be regarded as one-dimensional on the stellar surface. The timescale of the col-

lision between an ion and an electron is

$$t_{ie} = \frac{3(kT_e)^{1.5} m_e^{0.5}}{4\sqrt{2}\pi e^4 n_e \ln \bar{\Lambda}} \sim 10^7 \frac{\text{cm}^{-3}}{n_e} \text{ s}, \quad (3)$$

where  $\ln \bar{\Lambda}$  is a factor of  $\sim 10$  for the plasma atmosphere. Accounting the diffusion of the plasma, we have

$$-\nabla p - n_e e \mathbf{u} \times \mathbf{B} - \frac{m_e n_e \mathbf{u}}{t_{ie}} = m_e n_e \frac{d\mathbf{u}}{dt}, \quad (4)$$

where  $p$  is the pressure of the plasma,  $\mathbf{u}$  is the velocity of electrons and  $\mathbf{B}$  is the local magnetic field in a vertical direction. From Equation (4) the current density can be regarded as

$$\mathbf{J} = n_e \mathbf{u} = -\frac{D}{R} \frac{\partial n_e}{\partial \theta} \hat{\theta}, \quad (5)$$

where  $D$  is defined as the diffusion coefficient and  $\hat{\theta}$  the local orthogonal unit vectors in the directions of increasing.

Actually, there must be considered the ambipolar diffusion effect because the mass of ions is greater than that of electrons. For the two-temperature atmosphere, the ambipolar diffusion coefficient

$$D_A = \left(1 + \frac{T_i}{T_e}\right) \frac{kT_e t_{ie}}{m_e (1 + \omega_c^2 t_{ie}^2)}, \quad (6)$$

where  $\omega_c$  is Larmor frequency. Diffusion is blocked by a Lorentz force with a strong magnetic field near the polar cap. However, regarding as a dipole magnetic field, with the increase of  $\theta$ , collision between ions and electrons may play a leading role in blocking the diffusion against the magnetic field. Certainly, there are still small parts of none-strange ISM-accreted matter that could permeate into the interior of the star, i.e., penetrating the strangeness barrier. The penetration timescale of ions when there is a stable equilibrium between accretion and permeation for these falling ions is  $\tau_p \sim \Delta M / \dot{M}_X \sim 0.1 - 10^5 \text{ s}$  (Wang et al. 2017). As the electrons diffuse across magnetic field lines, spreading over almost the entire stellar surface with a low penetration, a stable diffusion equation can be described as

$$\frac{\partial n_e}{\partial t} = \frac{D_A}{R^2} \frac{1}{\sin \theta} \frac{\partial}{\partial \theta} \left( \sin \theta \frac{\partial n_e}{\partial \theta} \right) - \frac{n_e}{\tau_p}. \quad (7)$$

The solution of  $n_e$  can be well fitted by a single power law distribution at high latitude regions. The nonuniform toy model may predict multipole magnetic fields would be on the surface. Then, the accreted particles moves along with this magnetic fields into high latitude regions from polar caps.

Here, a typical diffused length of the particles which can diffuse over the whole stellar surface would be

$$L = \sqrt{D_A \tau_p} \gtrsim R. \quad (8)$$

With a number density of  $n_i \sim 10^{22} \text{ cm}^{-3}$  and  $R \sim 10 \text{ km}$ , one can infer that there is a weak magnetic field ( $10^8 \text{ G} \lesssim B \lesssim 10^{10} \text{ G}$ ) on the surface. In fact, XDINSs are radio quiet and show purely thermal X-ray emissions that suggests their magnetospheres may be not active. However, they are located in the upper right up of the  $P - \dot{P}$  diagram ( $B \sim 10^{12} - 10^{14} \text{ G}$ ) and beyond the death line to be “active” NSs. The reason why the real magnetic field is smaller than the  $P - \dot{P}$ -inferred magnetic field is that the propeller torque of a fallback disk may modify the period derivative (Liu et al. 2014). Additionally, there may be some diffusions

in the magnetosphere before ISM accreted into the stellar surface so that a weak magnetic field is estimated.

The X-ray optical thin atmosphere presents some faint absorption lines which may be derived from hydrocyclotron oscillation (Xu 2012) in spectra. These absorption lines can be well fitted by single gaussian absorptions with widths  $\sigma \sim 0.05 \text{ keV}$ , except J0720 shows a broad one ( $\sigma \gtrsim 1 \text{ keV}$ ). We also fit the spectrum of J0720 with the nonuniform model plus a power law emission. However, the fact of a high-energy tail is surprisingly close to a Wien spectrum (van Kerkwijk et al. 2007) that suggests the spectrum doesn’t have non-thermal (i.e., power law) components. Therefore, this broad line may be composed of multiple absorption lines.

A normal NS atmosphere is supposed to be on top of a condensed surface (Ho et al. 2007). However, the condensed surface is suggested to be maintained by a strong magnetic field ( $\sim 10^{13} \text{ G}$ , Lai 2001). In this case, some absorption features would be exhibited in the X-ray spectrum of J1856, but not detected with certainty. In addition, this condensed surface described as an additional “modified” black body (Ho et al. 2007), brings more low-energy photons so that it have to introduce a large value of  $N_H$  that would consequently present a strong photoelectric absorption. The spectral deviation, which is not an observation error, is unlikely to be originated from a uniform NS atmosphere. And the nonuniformity of the atmosphere which is demonstrated by the X-ray pulsation, can not be understood in the frame of some creating processes of NS atmosphere (e.g., Chang & Bildsten 2003).

### 4.3 Infrared observations of XDINS

Infrared (IR) observations are very important to understand the surroundings of NS (e.g., disks around isolated NSs, Wang et al. 2006, 2014). Accretion disks around magnetars are supported by X-ray spectral and timing observations, as well as in radio, optical, and IR observations (e.g., Trümper et al. 2013). Thus, XDINSs and magnetars which are rotating slowly as well as some high magnetic NSs are considered the most promising places to find fallback disks. Even the luminosities of XDINSs are less than that of magnetars, XDINSs might also have a comparable near IR emission (see, Figure 2 in Mignani et al. 2008).

An IR observation shows that dusty asteroid belts may surround J0806 and J2143 rather than thin dusty disks (Posselt et al. 2014). For the five other XDINSs, there are still not any significant evidence of warm or cold dust emission. A possible reason for the missing disks is that they never had disks since they were born or only small dust grains could close to the them just like they lost disks (Posselt et al. 2014). It is suggested that XDINSs may be during ISM-accreting which is parallel to Bondi accreting. However, the spherical accretion can not provide a strong braking torque during the stellar evolution. Also, Ertan et al. (2014) interpret that the Seven have gone through a past accretion phase with spin-down (i.e., the fall-back disk protruding into the NS’s magnetosphere) and emerged in their current state, with the X-ray luminosity provided by NS cooling and no longer by accretion. In case of the “transitional” disk, the IF radiation may be absorbed

by the geometrically thick disk that explains the evaporated thin disk.

For J2143, emission from a position of the NS is consisting of a blend of at least one southern and one brighter northern source in the red Photodetector Array Camera and Spectrometer (PACS; Poglitsch et al. 2010) band while it is very faint emission northwest of the NS in the blue PACS band (see, Figure 5 in Posselt et al. 2014). The belt as well as these “positional disturbances” may result in the flat spectrum at optical bands. Lo Curto et al. (2007) shows that the IR flux upper limits derived by *VLT* are well above the extrapolated X-ray spectrum. To better constrain the XDINSs’ optical/NIR emission properties, there still need much deeper observations. After around 5 years, the IR properties of XDINS would be detected by the Large Optical Telescope (LOT)

#### 4.4 Geometry of XDINS

A rotating NS with nonuniform plasma atmosphere could emit pulsed emissions which would be observed. In this case, the PF depends on the inclination angle  $\alpha$  (see Figure 6) which tends to align in the regime of the wind braking (Tong & Kou 2017). It is assumed that the discovered H $\alpha$  nebula (see van Kerkwijk & Kulkarni 2001b) is powered by a magnetic dipole braking, a roughly NS’s age of  $\sim 5 \times 10^5$  years is calculated for J1856 from its proper motion. Thus, as shown in pulsar  $P-\dot{P}$  diagram, there may be some evolution links between XDINSs and magnetars. For instance, J1856 may be in a state of wind brake before it shows purely thermal emission (Tong & Kou 2017). This may indicate that XDINS may be the result of a magnetar evolution (i.e., anti-magnetar which is radio-silent emitting X-ray).

To constrain the geometry of XDINS, the two angles ( $\alpha$  and  $\zeta$ ) could be calculated through measured pulsations and polarizations. The results of X-ray pulsation measurement are shown in Table 2 while the polarization in the soft X-rays are not feasible yet. However, X-ray polarized properties are very significant to detect NS’s magnetic field and constrain the surface (e.g., González Caniulef et al. 2016) as well as test the model presented in this paper. Moreover, both optical pulsations and polarization measurements are very difficult within reach for quite faint targets, like the Seven which have optical counterparts with magnitudes  $\sim 26 - 28$ . Only one of the seven, J1856, have been detected optical linear polarization (Mignani et al. 2017) which indicates a magnetic field  $B \sim 10^{13}$  G. While the properties of X-ray polarization may be different from that of optical polarization as a result of X-ray and optical emission come from different positions with different optical depth. The X-ray polarised properties are expected to be tested by the Lightweight Asymmetry and Magnetism Probe (LAMP), which is supposed to work on China’s space station around 2020 (She et al. 2015).

#### 5 SUMMARY

In this paper, we presented a radiative model of nonuniform plasma atmosphere on an emission-negligible strangeon star’s surface, and proposed that the observed emission is the bremsstrahlung radiation from the atmosphere. The ISM-accreted matter moves along the magnetic field lines to polar

caps, and may diffuse to other parts and makes the atmosphere nonuniform. This allows us to understand the spectral index deviation from the expected R-J spectrum and the X-ray pulsations as well as the optical/UV excess of XDINS. The spectra of five XDINSs (J0720, J0806, J1308, J1605 and J1856) would be well fitted in the radiative model, from X-ray to optical/UV bands, exhibiting gaussian like absorption lines. The results of data fitting show that the electron temperatures are  $\sim 100 - 200$  eV and that the radiation radii are  $\sim 5 - 14$  km.

#### ACKNOWLEDGEMENTS

We are grateful to Hao Tong at Guangzhou University for discussions. This work is supported by the National Natural Science Foundation of China (11673002, 11633004 and U1531243), the Strategic Priority Research Program (XDB23010200) and Frontier Science Key Project (QYZDJ-SSW-SLH017) of Chinese Academy of Sciences, and the Ministry of Science and Technology (2016YFE0100300).

#### REFERENCES

- Alcock, C., Farhi, E., & Olinto, A. 1986, *ApJ*, 310, 261
- Arnaud, K. A. 1996, *Astronomical Data Analysis Software and Systems V*, 101, 17
- Burwitz, V., Zavlin, V. E., Neuhäuser, R., Predehl, P., Trümper, J., & Brinkman, A. C. 2001, *A&A*, 379, L35
- Burwitz, V., Haberl, F., Neuhäuser, R., Predehl, P., Trümper, J., & Zavlin, V. E. 2003, *A&A*, 399, 1109
- Cardelli, J. A., & Ackerman, T. P. 1983, *Publ. Astron. Soc. Pac.* 95, 451
- Chang, P., & Bildsten, L. 2003, *ApJ*, 585, 464
- Chatterjee, P., Hernquist, L., & Narayan, R. 2000, *ApJ*, 534, 373
- Davidson, K., & Ostriker, J. P. 1973, *ApJ*, 179, 585
- Drake, J. J., et al. 2002, *ApJ*, 572, 996
- Ertan, Ü., Çalıskan, Ş., Benli, O., & Alpar, M. A. 2014, *MNRAS*, 444, 1559
- Ertan, Ü., Çalıskan, Ş., & Alpar, M. A. 2017, *MNRAS*, 470, 1253
- Geppert, U., Küker, M., & Page, D. 2006, *A&A*, 457, 937
- Goldreich, P., & Julian, W. H. 1969, *ApJ*, 157, 869
- González Caniulef, D., Zane, S., Taverna, R., Turolla, R., & Wu, K. 2016, *MNRAS*, 459, 3585
- Haberl, F., Zavlin, V. E., Trümper, J., & Burwitz, V. 2004, *A&A*, 419, 1077
- Haberl, F. 2007, *Ap&SS*, 308, 181
- Haensel, P. 2001, *A&A*, 380, 186
- Ho, W. C. G., Kaplan, D. L., Chang, P., van Adelsberg, M., & Potekhin, A. Y. 2007, *MNRAS*, 375, 821
- Illarionov, A. F., & Sunyaev, R. A. 1975, *A&A*, 39, 185
- Kalberla, P. M. W., Burton, W. B., Hartmann, D., et al. 2005, *A&A*, 440, 775
- Kaplan, D. L., & van Kerkwijk, M. H. 2005, *ApJ*, 635, L65
- Kaplan, D. L., & van Kerkwijk, M. H. 2009, *ApJ*, 705, 798
- Kaplan, D. L., Kamble, A., van Kerkwijk, M. H., & Ho, W. C. G. 2011, *ApJ*, 736, 117
- Kondratiev, V. I., McLaughlin, M. A., Lorimer, D. R., Burgay, M., Possenti, A., Turolla, R., & Popov, S. B. 2009, *ApJ*, 702, 692
- Lai, D. 2001, *RvMP*, 73, 629
- Lai, X., & Xu, R. 2017, *Journal of Physics: Conf. Series* 861, 012027
- Lo Curto, G., Mignani, R. P., Perna, R., & Israel, G. L. *A&A*, 2007, 473, 539



- Liu, X. W., Xu, R. X., Qiao, G. J., Han, J. L., & Tong, H. 2014, RAA, 14, 85
- Menou, K., Esin, A. A., Narayan, R., et al. 1999, ApJ, 520, 276
- Mignani, R. P., Falomo, R., Moretti, A., Treves, A., Turolla, R., Sartore, N., Zane, S., Arcidiacono, C., Lombini, M., Farinato, J., Baruffolo, A., Ragazzoni, R., & Marchetti, E. 2008, A&A, 488, 267
- Mignani, R. P., Testa, V., González Caniulef, D., et al. 2017, MNRAS, 465, 492
- Mori, K., & Ruderman, M. A. 2003, ApJ, 592, L75
- Morrison, R., & McCammon, D. 1983, ApJ, 270, 119
- Poglitsch, A., Waelkens, C., Geis, N., et al. 2010, A&A, 518, L2
- Pons, J. A., Miralles, J. A., & Geppert, U. 2009, A&A 496, 207
- Posselt, B., Pavlov, G. G., Popov, S., & Wachter, S. 2014, ApJS, 215, 3
- Potekhin, A. Y., Ho, W. C. G., & Chabrier, G. 2016, arXiv:1605.01281
- Predehl, P., & Schmitt, J. H. M. M. 1995, A&A, 293, 889
- Romanova, M. M., Blinova, A. A., Ustyugova, G. V., Koldoba, A. V., & Lovelace, R. V. E. 2017, arXiv:1704.08336
- Romanova, M. M., Toropina, O. D., Toropin, Y. M., & Lovelace, R. V. E. 2003, ApJ, 588, 400
- She, R., Feng, H., Muleri, F., et al. 2015, Proc. SPIE, 9601, 96010I
- Suleimanov, V., Hambaryan, V., Potekhin, A. Y., et al. 2010, A&A, 522, A111
- Tong, H. 2016, Science China Physics, Mechanics & Astronomy, 59, 1
- Tong, H., & Kou, F. F. 2017, ApJ, 837, 117
- Toropina, O. D., Romanova, M. M., Toropin, Yu. M., & Lovelace, R. V. E. 2001, ApJ, 561, 964
- Trümper, J. E., Burwit, V., Haberl, F., & Zavlin, V.E. 2004, Nuclear Physics B Proceedings Supplements, 132, 560
- Trümper, J. E., Dennerl, K., Kylafis, N. D., Ertan, Ü., & Zezas, A. 2013, ApJ, 764, 49
- Turolla, R. 2009, Astrophysics and Space Science Library, 357, 141
- Usov, V. V., 2001, ApJ, 550, L179
- van Kerkwijk, M. H., & Kaplan, D. L. 2007, Astrophys Space Sci, 308, 191
- van Kerkwijk, M. H., Kaplan, D. L., Pavlov, G. G., & Mori, K. 2007, ApJ, 659, L149
- van Kerkwijk, M. H. & Kulkarni, S. R. 2001a, A&A, 378, 986
- van Kerkwijk, M. H., & Kulkarni, S. R. 2001b, A&A, 380, 221
- Wang, W. Y., Lu, J. G., Tong, H., Ge, M. Y., Li, Z. S., Men, Y. P., & Xu, R. X. 2017, ApJ, 837, 81
- Wang, Z., Chakrabarty, D., & Kaplan, D. L. 2006, Nature, 440, 772
- Wang, Z., Ng, C. -Y., Wang, X., Li, A., & Kaplan, D. L. 2014, ApJ, 793, 8
- Xu, R. X. 2002, ApJ, 570, L65
- Xu, R. X. 2003, ApJ, 596, L59
- Xu, R. X. 2014, Research in Astron. Astrophys, 14, 617
- Xu, R. X., Bastrukov, S. I., Weber, F., Yu, J. W., & Molodtsova, I. V. 2012, PhRvD, 85, 023008
- Zane, S., Turolla, R. 2006, MNRAS, 366, 727

## 6 APPENDIX: FLUX OF THE BREMSSTRAHLUNG FROM A ROTATING NS

In the corotating coordinate frame  $(x, y, z)$ ,  $\mathbf{P} [\mathbf{P}=(\theta, \phi)$ , unit vector  $\mathbf{n}$ ] is the emission point on the NS's surface, two angles  $\zeta$  and  $\alpha$  are defined: the former is the angle between the line of sight (LOS) and the spin axis  $\Omega_s$  which is in the  $\hat{x}\hat{z}$ -plane, where  $z$ -axis parallel to the magnetic (dipole) axis, while the latter is the inclination angle that between

the magnetic axis (a dipole magnetic field is assumed) and the spin axis. Also, a fixed coordinate system is introduced,  $(X, Y, Z)$  with the  $Z$ -axis parallel to LOS and the  $X$ -axis in the LOS-spin plane. The associated polar angles are  $(\Theta_s, \Phi_s)$  in the fixed coordinate, respectively. The transformations linking the pairs of polar angles in the two systems are (see, [Zane & Turolla 2006](#))

$$\begin{cases} \cos \theta = \mathbf{n} \cdot \mathbf{b} \\ \cos \phi = \mathbf{n}_\perp \cdot \mathbf{q}_\perp, \end{cases} \quad (9)$$

where  $\mathbf{n} = (\sin \Theta_s \cos \Phi_s, \sin \Theta_s \sin \Phi_s, \cos \Phi_s)$ ,  $\mathbf{b} = (\sin \zeta \cos \alpha - \cos \zeta \sin \alpha \cos \omega t, \sin \alpha \sin \omega t, \cos \zeta \sin \alpha + \sin \zeta \cos \alpha \cos \omega t)$  is the magnetic axis in the fixed frame (here  $\omega = 2\pi/P$  is the angular velocity), an additional vector  $\mathbf{q} = (-\cos \zeta \cos \omega t, \sin \omega t, \sin \zeta \cos \omega t)$ , the component of  $\mathbf{q}$  perpendicular to  $\mathbf{b}$

$$\mathbf{q}_\perp = \frac{\mathbf{q} - (\mathbf{b} \cdot \mathbf{q})\mathbf{b}}{(1 - \mathbf{b} \cdot \mathbf{q})^{\frac{1}{2}}}, \quad (10)$$

and  $\mathbf{n}_\perp$  is defined in analogy with  $\mathbf{q}_\perp$ .

The emission from a local region of a rotating NS is shown in Figure 6. Its long timescale  $T$  averaged flux of the radiation could be described as

$$\bar{F}_\nu = \frac{1}{T} \int_0^T dt \int I_\nu \cos \Theta_s d\Omega, \quad (11)$$

where  $I_\nu$  is the specific intensity and  $d\Omega$  is the solid angle in the fixed coordinate. In the following calculations, it is assumed that the density of the strangeon star is  $1.5 \times 2.8 \times 10^{14} \text{ cm}^{-3}$  and the atmosphere is mainly composed of hydrogens ( $m_i \sim 1 \text{ GeV}/c^2$ ). The observed time averaged radiation should be gravitationally red-shifted, i.e.,

$$\bar{F}_\nu^\infty \simeq F_{\nu 0} + \pi \left( \frac{R_{\text{opt}}^\infty}{d} \right)^2 \frac{B_\nu}{T} \int_0^T dt \int [1 - \exp(-\tau_\nu^\infty)] d\Omega, \quad (12)$$

where  $R_{\text{opt}}^\infty$  is the radiation radius,  $d$  is the distance from the source,  $B_\nu$  is the Planck function,  $F_{\nu 0}$  is the flux from a bare strangeon star which can be calculated to be

$$\pi \left( \frac{R_{\text{opt}}^\infty}{d} \right)^2 \frac{B_\nu}{T} \exp(-\tau_\nu^\infty) \int_0^T dt \int [1 - \exp(-\tau_\nu^\infty)] d\Omega, \quad (13)$$

and  $\tau_\infty(\nu)$  is the observed optical depth at far field which can be described as

$$\begin{aligned} \tau_\infty(\nu) &= \frac{8\pi\sqrt{2}h^2n_{i0}^2(\theta)e^6kT_i}{3m_e^{1.5}(h\nu)^{3.5}m_i g c} [1 - \exp(-\frac{h\nu}{kT_e})] \\ &= 3.92 \times 10^{-45} \frac{n_{i0}^2(\theta)(kT_i)_{\text{keV}}}{(h\nu)_{\text{keV}}^{3.5} R_{\text{km}}} [1 - \exp(-\frac{h\nu}{kT_e})], \end{aligned} \quad (14)$$

where  $h$  is the Planck constant,  $m_e$  is the mass of a electron,  $T_e$  is the temperature of electrons,  $e$  is elementary charge and  $c$  is the speed of light.

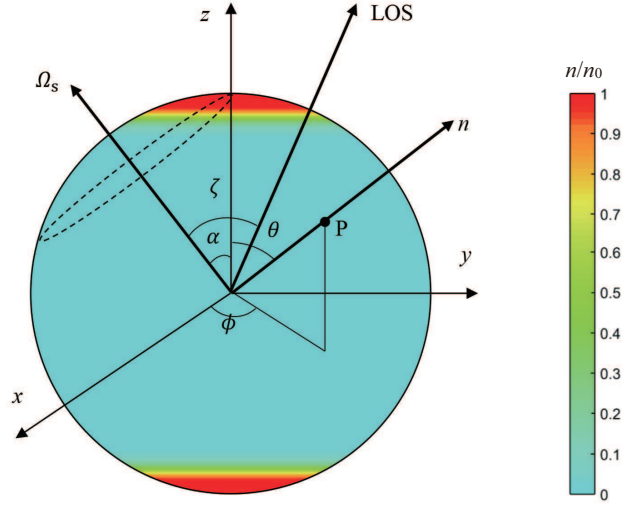


**Figure 6.** Coordinate axes and angles used to describe the geometry and pulsed emission as well as the distribution by colour of the plasma atmosphere number density. The dashed line indicates the position of the magnetic pole  $\mathbf{b}$  as the NS rotates about  $\Omega_s$ . The parameters of the colored electrons' number density are  $\xi = 150, \gamma = 3$ .